DOI: 10.1002/ejic.201100313

Resolving Composition and Structure of *RE*–Sb–O–C Natural Superlattice Phases (*RE* = La, Ho)

Peng Wang,[a] Scott Forbes,[a] Volodymyr Svitlyk,[b] Ashur Aushana,[c] and Yurij Mozharivskyj*[a]

Dedicated to Professor John D. Corbett on the occasion of his 85th birthday

Keywords: Solid-state structures / Solid-phase synthesis / Rare earths

A family of rare earth antimonide oxycarbides have been prepared and structurally characterized. These superlattice phases are constructed from NaCl-type *RE*Sb slabs sandwiched between *RE*–O–C layers. Depending on the carbon content and synthetic conditions, three different *RE*–Sb–O–C structures can be obtained. At lower temperatures, $RE_{9-\delta}Sb_5(O,C)_5$ phases are obtained for *RE* = La, Ho. These phases adopt a stuffed Sc_2Sb-type structure with *P*4/*nmm* symmetry. An O/C mixture, in which the O/C ratio is larger than 4:1, is randomly distributed within the *RE*–O–C layers. The *RE* atoms are highly disordered within the oxide layer. At temperatures above the melting point of the samples, $RE_9Sb_5O_4C$ phases with *P*4/*n* symmetry are produced. The *RE*–O–C layers in $RE_9Sb_5O_4$ are fully ordered; the *RE* sites are well defined, and the O and C atoms occupy the tetrahedral and square-pyramidal voids, respectively. At high temperatures, a new ordered $La_{14}Sb_8O_7C$ structure with *P*4*bm* symmetry was discovered. The $La_{14}Sb_8O_7C$ phase is structurally similar to $RE_9Sb_5O_4C$ and features ordered arrangements of La and O/C atoms in the La–O–C layer. The $RE_{9-\delta}Sb_5(O,C)_5$, $RE_9Sb_5O_4C$ and $La_{14}Sb_8O_7C$ phases appear to be charge-balanced, and their compositions and structures are controlled by the O/C ratio. Parallel preparative experiments revealed the importance of carbon in the formation of these layered phases. In addition, it has been established that the purity of the rare earth metals influences the compositions and structures of the products.

Introduction

Recently, a new approach known as the natural superlattice approach[1] has been employed in the design and preparation of new materials for thermoelectric applications. An ideal thermoelectric material must have a large Seebeck coefficient α and a low thermal conductivity κ, while retaining a high electrical conductivity δ.[2] These desired physical properties, however, are rarely found simultaneously in a single homogeneous material. By constructing a natural superlattice, a material with desired electrical properties is combined with a thermally insulating material in such a way that both of their basic structural building blocks are preserved and interwoven into a single structure.[3] Such structural design has been realized in the $Ca_xYb_{1-x}Zn_2Sb_2$ phases.[4] The structure of the $Ca_xYb_{1-x}Zn_2Sb_2$ system consists of two alternating layers: the cationic Ca^{2+}/Yb^{2+} layer and the anionic $Zn_2Sb_2^{2-}$ layer. Thermoelectric performance is improved as the disordered cationic layer functions as a phonon barrier to reduce the thermal conductivity, whereas the electrical properties of the anion layer remain unperturbed.

Inspired by the natural superlattice approach, we have undertaken systematic structural and compositional analyses of the partially oxidized rare earth antimonide oxides $RE_9Sb_5O_5$ (*RE* = La, Ho).[5–7] Previous works[5–7] have revealed some interesting structural features of these compounds. As shown in Figure 1, their structure can be understood as a variant of the Sc_2Sb structure.[6] The unit cell of Sc_2Sb consists of a layer of Sc atoms sandwiched between slightly puckered NaCl-type ScSb slabs. In the case of the $RE_9Sb_5O_5$ phases, the unit cells consist of $[RE_4O_5]$ layers and NaCl-type $[RE_5Sb_5]$ slabs. The oxide layer has four *RE* atoms occupying four out of five metal positions present in the Sc_2Sb structure, and the oxygen atoms fill the interstitial sites.[5]

The $[RE_5Sb_5]$ slabs in the $RE_9Sb_5O_5$ system are expected to retain the electrical properties of the *RE*Sb binaries as they share the same structure. The pristine *RE*Sb binaries are semimetallic/metallic materials[8] containing some of the heaviest elements in the periodic table. These binary phases,

[a] Department of Chemistry and Chemical Biology, McMaster University,
1280 Main Street West, Hamilton, Ontario L8S 4M1, Canada
[b] European Synchrotron Radiation Facility,
6 rue Jules Horowitz, P. B. 220, 38043 Grenoble, France
[c] Department of Chemistry, York University,
4700 Keele Street, Toronto, Ontario M3J 1P3, Canada
Supporting information for this article is available on the WWW under http://dx.doi.org/10.1002/ejic.201100313.

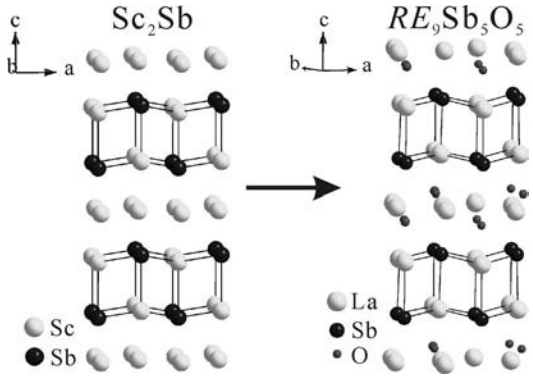

Figure 1. Structures of Sc_2Sb and $RE_9Sb_5O_5$.

adopting a simple NaCl-type crystal structure, are expected to possess a relatively high thermal conductivity due to the small number of atoms in their unit cells.[9,10] The $[RE_4O_5]$ layer sandwiched between two $[RE_5Sb_5]$ slabs adopts a completely different structure and is expected to perturb phonon propagation by increasing the structural complexity.

It was also noticed that there are two dissimilar oxygen positions within the RE_4O_5 layer. One of the sites (8*g*) is surrounded by four neighboring rare earth elements in a tetrahedral arrangement, whereas the other (2*c*) has a rather unusual square-pyramidal arrangement surrounded by five *RE* atoms. With oxygen atoms fully occupying the two sites, the electron-rich formula $RE_9Sb_5O_5$ $[RE^{3+}{}_9Sb^{3-}{}_5O^{2-}{}_5(2e^-)]$ results. An electron-balanced formula $RE_9Sb_5O_4C$ ($RE^{3+}{}_9Sb^{3-}{}_5O^{2-}{}_4C^{4-}$), in which C replaces oxygen in the 2*c* site, was also suggested;[6] however, the electrical resistivity measurements performed on the bulk samples revealed a metallic-type behavior, thus supporting the electron-rich model.

The metallic-type conductivity implies that the $RE_9Sb_5O_5$ phases would possess a low thermopower α, unattractive for industrial applications. Nonetheless, the observed electrical properties may also result from a partial substitution of C in the 2*c* site by O (if the 2*c* site is assumed to be primarily occupied by C). The refinement results for the $RE_9Sb_5O_5$ single crystals[6] yielded large thermal vibrations for the 2*c* oxygen atoms, suggesting the presence of a lighter element at this site. The existence of pure $RE_9Sb_5O_5$ may also be questionable considering the existence of the semiconducting RE_3SbO_3 and $RE_8Sb_{3-\delta}O_8$ antimonide oxides, in which oxygen atoms have a typical tetrahedral *RE* environment.[11] The RE_3SbO_3 phases are produced by direct high-temperature fusion of the *RE*Sb and RE_2O_3 binaries, whereas $RE_8Sb_{3-\delta}O_8$ can be derived from RE_3SbO_3 through the loss of *RE* and oxygen.

Considering the above-discussed factors, it is likely that "$RE_9Sb_5O_5$" is stabilized by light elements other than oxygen. If a C atom can replace the O atom in the 2*c* site in "$RE_9Sb_5O_5$", the electrical properties could be adjusted to render these phases semiconducting and in favor of good thermoelectric performance. This work focuses on the synthesis, compositions, and structural characterization of phases related to the $RE_9Sb_5O_5$/$RE_9Sb_5O_4C$ (*RE* = La, Ho) phases. The early rare earth element La was chosen for this investigation to establish a connection to previous studies. Ho was selected to expand the series and to allow a comparison of the early and late rare earth systems. The aim of this work was also to uncover the significance of carbon on the structural, chemical, and physical properties of these phases.

Results and Discussion

The experimental results revealed interesting compositional and structural features as well as relationships between the various phases. Percentage yield (in wt.-%) of the desired phase in the bulk samples is plotted against the loaded amount of carbon in Figure 2. The products are identified by their crystal structures. The different symbols represent the purity of the La and Ho metals and annealing conditions (table in Figure 2). For $x = 0$ (no carbon added), the samples were prepared from commercial and purified La and Ho. The graph in Figure 2 reveals two trends: (1) the yield of the product depends on the carbon content in the starting material; and (2) the synthetic conditions determine the structure of the products. To explain the observed trends, the crystal structure and composition of each phase need to be discussed.

$RE_9Sb_5O_4C$

According to the single-crystal X-ray diffraction analysis, the $La_9Sb_5O_4C$ and $Ho_9Sb_5O_4C$ phases adopt an $La_9Sb_5O_5$-type structure with the *P*4/*n* space group. As discussed in the Introduction, in the $La_9Sb_5O_5$ structure, oxygen atoms occupy both the tetrahedral (8*g*) and square-pyramidal (2*c*) interstitial sites. The $La_9Sb_5O_5$ model was used to refine the $La_9Sb_5O_4C$ and $Ho_9Sb_5O_4C$ structures; however, it was observed that the thermal parameters of the oxygen atoms in the 2*c* site were abnormally large in comparison with those of the 8*g* oxygen atom. A modified model (Figure 3) with carbon instead of oxygen atoms at the 2*c* site was tried. In the new model, the thermal vibration parameters for the 2*c* site were significantly improved (Table 1), whereas other atomic parameters remained unaffected. As a result, the compositions of the La and Ho phases were assumed to be $La_9Sb_5O_4C$ and $Ho_9Sb_5O_4C$, respectively.

In addition to the refinement results, other factors support carbon rather than oxygen in the square-pyramidal interstitial 2*c* site defined by five *RE* atoms. For example, in the rare earth dicarbides REC_2[12,13] with the CaC_2 structure, the carbon atoms have five *RE* atoms in their first coordination sphere, similar to the 2*c* site environment in $RE_9Sb_5O_4C$. It has to be emphasized that in REC_2, the square-pyramidal RE_5C units share square faces, which results in short C–C bonds, but no such C–C bonds are present in $RE_9Sb_5O_4C$. In the RE_2O_3 oxides, oxygen atoms re-

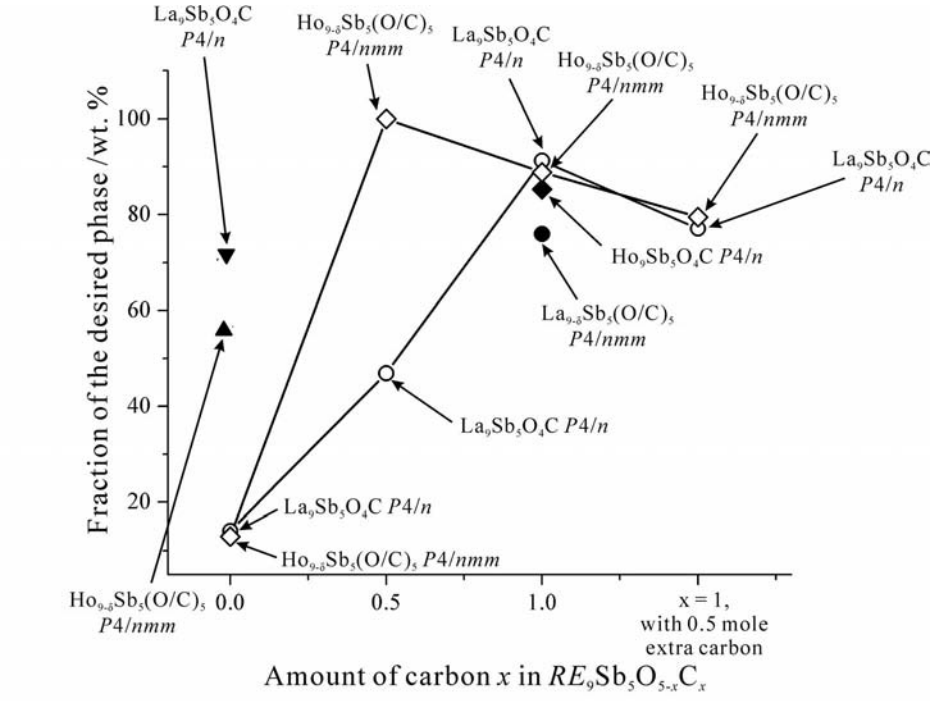

Symbol	Formula	Temperature	Starting Material
—○—	$La_9Sb_5O_{5-x}C_x$	1550°C	with purified La
●	$La_9Sb_5O_{5-x}C_x$	1400°C	with purified La
▼	$La_9Sb_5O_{5-x}C_x$	1550°C	with commercial La
—◇—	$Ho_9Sb_5O_{5-x}C_x$	1650°C	with purified Ho
◆	$Ho_9Sb_5O_{5-x}C_x$	1575°C	with purified Ho and Ho_5Sb_3 flux
▲	$Ho_9Sb_5O_{5-x}C_x$	1650°C	with commercial Ho

Figure 2. Yield of the desired phases in each sample plotted against the amount of added carbon.

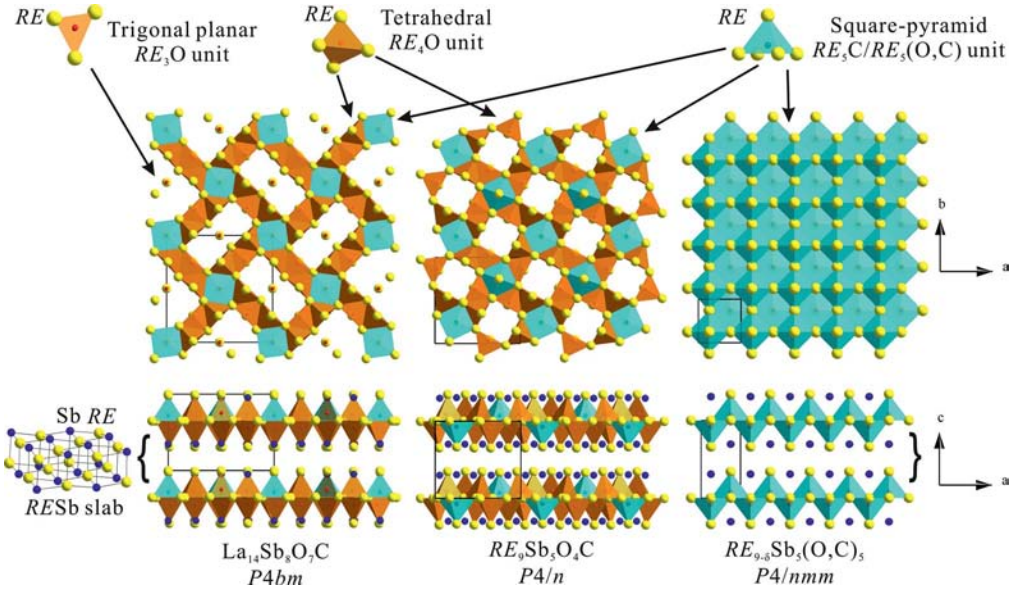

Figure 3. Crystal structures of $La_{14}Sb_8O_7C$, $RE_9Sb_5O_4C$, $RE_{9-\delta}Sb_5(O,C)_5$ and their building blocks.

Table 1. Thermal parameters of the O/C atoms in the 2*c* square-pyramidal sites and resulting R_1 values in the $RE_9Sb_5O_5$/$RE_9Sb_5O_4C$ models.

Refined composition	Atom on 2*c* site	U_{eq}	R_1 value
$La_9Sb_5O_5$	O	0.024(5)	0.0531
$La_9Sb_5O_4C$	C	0.011(4)	0.0531
$Ho_9Sb_5O_5$	O	0.050(8)	0.0264
$Ho_9Sb_5O_4C$	C	0.016(6)	0.0263

side inside the *RE* tetrahedra,[14] and this environment is analogous to that of the 8*g* oxygen site in $RE_9Sb_5O_4C$.

The bond valence sum method[15] has been employed to test site preferences in the $La_9Sb_5O_4C$ and $Ho_9Sb_5O_4C$. The Ho–C R_0 parameter was derived from the bond lengths and coordination geometry of Ho_2C,[16] in which carbon is assumed to be tetravalent. Unfortunately, the R_0 parameter for the La–C bond could not be extracted as no comparable compound exists. The R_0 parameters for the La–O and Ho–O bonds were taken from the work by Brese et al.[17] The calculated bond valence (B-V) sums for both oxygen and carbon in the 2*c* site are listed in Table 2. The results suggest the presence of a carbon atom in the 2*c* site, in agreement with the X-ray structural analysis results.

Table 2. Bond valence sum values for atoms in the 2*c* site.

Atom in 2*c* site	R_0 value	Expected B-V sum	Calculated B-V sum
		$La_9Sb_5O_4C$	
O	2.172 Å	2	1.693
C	–	4	–
		$Ho_9Sb_5O_4C$	
O	2.023 Å	2	1.801
C	2.318 Å	4	3.997

$RE_{9-\delta}Sb_5(O,C)_5$

Similar to the $RE_9Sb_5O_4C$ structure, the $RE_{9-\delta}Sb_5(O,C)_5$ structure also consists of an *RE*–O–C layer sandwiched between NaCl-type *RE*Sb slabs. Initially, the $RE_{9-\delta}Sb_5(O,C)_5$ crystals were solved in the Sc_2Sb structure, with full *RE* occupancies and O/C atoms filling the interstitial sites between the *RE*Sb slabs. During the refinement, the *RE*(2) metal atoms in the 2*a* position (¾,¼,0) in the *RE*–O–C layer exhibited large disk-shaped thermal ellipsoids in the *ab*-plane. Structural refinement of the low-temperature (100 K) data of the $La_{9-\delta}Sb_5(O,C)_5$ crystal suggested two alternative models, with the *RE*(2) atoms having either an 8*i* or 8*g* position. The new models yielded improved *RE*(2) thermal parameters and lower *R* values both for $La_{9-\delta}Sb_5(O,C)_5$ and $Ho_{9-\delta}Sb_5(O,C)_5$. The structural model with the *RE*(2) atoms in the 8*i* site yielded the lowest *R* values and reasonable thermal parameters for both the *RE*(2) and interstitial O/C(1) atoms; therefore, it is believed to be the best representation of the overall structure (comparison of the different models is given in the Supporting Information).

The *RE* deficiencies were always present irrespective of the model chosen, and thus the general formula for these phases is given as $RE_{9-\delta}Sb_5(O,C)_5$ [the refined compositions were $La_{8.80(1)}Sb_5(O,C)_5$ and $Ho_{8.84(4)}Sb_5(O,C)_5$]. During the refinement, the atomic site occupancy of the *RE*(2) atom and the thermal vibration parameters of the C/O atoms in the *RE*–O–C layers were correlated and, as a result, the *RE* occupation and O/C ratio could not be refined simultaneously. Another interesting outcome is that the O/C ratio in $RE_{9-\delta}Sb_5(O,C)_5$ is larger than in $RE_9Sb_5O_4C$ and likely leads to the *RE* deficiencies as oxygen is divalent and carbon is tetravalent. The larger O/C ratio also follows from the synthesis of the $Ho_9Sb_5O_{4.5}C_{0.5}$ sample, which yielded the $RE_{9-\delta}Sb_5(O,C)_5$ phase with high purity (Figure 2, x = 0.5, open diamonds).

Since the *RE*(2) disorder might be indicative of a superstructure, we decided to check for superstructure reflections. Analysis of the reciprocal space of the room-temperature diffraction data both for $La_{8.80(1)}Sb_5(O,C)_5$ and $Ho_{8.84(4)}Sb_5(O,C)_5$ revealed no signs of a superstructure. At 100 K, however, streaks of weak diffused spots were observed along the *c*-direction in the reciprocal space of $La_{8.80(1)}Sb_5(O,C)_5$ (see the Supporting Information). Such diffused scattering can imply some degree of ordering on the 8*i* site. From a structural perspective, the *RE*(2) disorder on the 8*i* site allows the *RE* environment around the O/C atoms to change from square-pyramidal into distorted tetrahedral (Figure 4). Such a change may be preferred if a particular site is occupied by oxygen. On the other hand, absence of the distortion, that is, retention of the *RE* square-pyramidal environment, can be associated with the presence of a carbon atom. It is difficult to establish what factors cause the *RE*(2) disorder: the absence of the O/C ordering, the O/C ratio, which is incommensurate with the atomic ordering and prevents it, or other parameters.

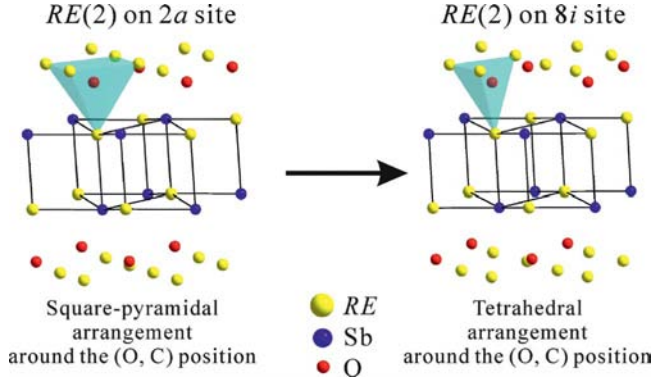

Figure 4. Structural models of $RE_{9-\delta}Sb_5(O,C)_5$ with *RE*(2) atoms in the 2*a* and 8*i* sites. The possible metal environments around the oxygen interstitial sites are identified with the polyhedra.

$La_{14}Sb_8O_7C$

The $La_{14}Sb_8O_7C$ structure also consists of NaCl-type LaSb slabs and La–O–C layers, but it possesses a larger unit cell with *P*4*bm* symmetry. The LaSb slabs of $La_{14}Sb_8O_7C$

are similar to those of $La_9Sb_5O_4C$, but there are four rather than two C/O sites in the La–O–C layer. The O1 and O2 sites have tetrahedral environments typical for oxygen atoms in this family of compounds; therefore, these sites are assumed to be fully occupied by oxygen atoms. The carbon site has a square-pyramidal La coordination, which is similar to that observed in $RE_9Sb_5O_4C$. The single-crystal structural refinement performed against all collected reflections yielded a smaller temperature factor on the carbon site in comparison with that of the tetrahedrally coordinated oxygen atoms. The thermal vibration of the carbon atom, however, became normal when the structural model was refined against high-angle reflections ($2\theta > 30°$). Whereas some oxygen atoms can be present, based on the structural analogy to $La_9Sb_5O_4C$, we believe that this site is predominantly occupied by carbon atoms. There is also an additional oxygen site (O3), which has only three neighboring La atoms in the trigonal-planar arrangement. A similar oxygen environment has also been observed in the $RE_8Sb_{3-\delta}O_8$ structures.[11]

Structural and Compositional Relationships

The common building blocks of the $RE_{9-\delta}Sb_5(O,C)_5$, $RE_9Sb_5O_4C$, and $La_{14}Sb_8O_7C$ structures are NaCl-type *RE*Sb slabs and *RE*–O–C layers. Although the NaCl-type *RE*Sb slabs remain identical among the three structures, the *RE*–O–C layers are different. The arrangement and ordering of the *RE* and O/C atoms within these layers appear to dictate the unit cell size as well as its symmetry. The $RE_9Sb_5O_4C$ structure can be viewed as a parent structure in this series. As discussed in the Introduction, this structure itself is a derivative of the Sc_2Sb structure in which the *RE* layer, sandwiched between *RE*Sb slabs, is deficient. Another difference to the Sc_2Sb structure is that the tetrahedral and square-pyramidal voids between the *RE* layer and the *RE*Sb slabs in $RE_9Sb_5O_4C$ are filled with oxygen and carbon atoms, respectively. A more detailed description of the $Sc_2Sb/RE_9Sb_5O_4C$ relationship can be found in the work by Nuss et al.[6] One interesting point is that the stoichiometric $RE_9Sb_5O_4C$ phases are charge-balanced. This fact may explain the "deficiency" of the *RE* layer, as compared with the Sc_2Sb structure, and the overall phase composition. The NaCl-type $(RE^{+3})_5(Sb^{-3})_5$ slab (composition is per formula unit) is charge-balanced, so the $(O^{-2})_4C^{-4}$ composition of the *RE*–O–C layer requires the presence of only four *RE* atoms to maintain the charge neutrality. This reduces the overall *RE*/Sb ratio from 2:1 expected for the Sc_2Sb-type structures to 1.8:1. The arrangement of the *RE* atoms is such that the square voids are created in the *RE*–O–C layers and, in addition, two types of interstitial voids, tetrahedral and square-pyramidal, are formed with the neighboring *RE*Sb slabs.

The $RE_{9-\delta}Sb_5(O,C)_5$ phases can be considered as derivatives of $RE_9Sb_5O_4C$, in which the carbon content is reduced. Such a reduction would lead to a decrease in the *RE* concentration within the *RE*–O–C layer, even if the carbon loss is offset by the equiatomic oxygen gain. Due to the different coordination requirements of oxygen and carbon atoms, the ordered atomic arrangement within the *RE*–O–C layer can be achieved only for specific *RE* and O/C stoichiometries. Whereas this condition is met in $RE_9Sb_5O_4C$, it is apparently not satisfied in $RE_{9-\delta}Sb_5(O,C)_5$. As a result, the *RE*–O–C layer of $RE_{9-\delta}Sb_5(O,C)_5$ contains both the *RE* disorder and the O/C statistical mixtures. On the local level, both of these features provide suitable environments for the oxygen and carbon atoms. Although we could not pinpoint the boundaries for the O/C ratio, based on the structural analysis and synthetic results, it appears that ratios $4:1 < O/C \leq 9:1$ are possible for $RE_{9-\delta}Sb_5(O,C)_5$.

The O/C ratio of 7:1 is of particular interest as it yields the $La_{14}Sb_8O_7C$ structure. As expected from the O/C ratio, the La–O–C layer is depleted in La (compared with $La_9Sb_5O_4C$) to maintain the charge balance. Interestingly, the La–O–C layer with the La_6O_7C composition now finds an atomic arrangement, which provides both the La ordering as well as proper environments for the oxygen and carbon atoms. When compared with $RE_9Sb_5O_4C$, the La layer in $La_{14}Sb_8O_7C$ has larger voids that can be viewed as two square voids from $RE_9Sb_5O_4C$ joined together. Since the $La_{14}Sb_8O_7C$ phase could not be prepared in bulk, and a similar $Ho_{14}Sb_8O_7C$ could not be verified to exist, it can be assumed that even small deviations from the 7:1 O/C ratio results in the formation of the $RE_{9-\delta}Sb_5(O,C)_5$-type phases.

Role of Temperature

For the same loading composition, the structure of the resulting phase depends on the annealing temperature. If the temperature is high enough to melt the samples, the resulting structure is $La_{14}Sb_8O_7C$ (*P*4*bm*) or $RE_9Sb_5O_4C$ (*P*4/*n*) with fully ordered *RE*–O–C layers. If the temperature is below the sample's melting point, however, the resulting structure is $RE_{9-\delta}Sb_5(O,C)_5$ (*P*4/*nmm*) with disordered *RE*–O–C layers. This trend can be clearly seen both for the $La_9Sb_5O_4C$ and $Ho_9Sb_5O_4C$ samples prepared from the distilled metals (Figure 2). If the $La_9Sb_5O_4C$ sample is annealed at 1400 °C, which is below its melting point, the major phase is $La_{9-\delta}Sb_5(O,C)_5$ (*P*4/*nmm*) (76 wt.-%, Figure 2, full sircles). But the same sample heated to 1550 °C, above its melting point, contains more than 90 wt.-% of the $La_9Sb_5O_4C$ (*P*4/*n*) phase (Figure 2, $x = 1$, open circles) without any traces of the $La_{9-\delta}Sb_5(O,C)_5$ phase. The $Ho_9Sb_5O_4C$ sample could not be melted at 1650 °C, which is the highest temperature currently achievable with our experimental setup; at this temperature, the major phase was $Ho_{9-\delta}Sb_5(O,C)_5$ (*P*4/*nmm*) (ca. 88 wt.-%, Figure 2, $x = 1$, open diamonds). Melting of the $Ho_9Sb_5O_4C$ sample was achieved by adding a 0.3 molar fraction of Ho_5Sb_3, which acted as a low-temperature flux. After melting the sample, the major phase was $Ho_9Sb_5O_4C$ (*P*4/*n*, 85 wt.-%, Figure 2, full diamonds). These experiments suggest that there is a large energy barrier for the atomic ordering within the *RE*–O–C layers, and a full ordering is achieved only from the liquid state.

Impact of Carbon and Purity of RE Elements

One can argue that the evidence from the structural refinement may not be sufficient to fully support the $RE_9Sb_5O_4C$ composition. In addition, the X-ray diffraction studies on the $RE_{9-\delta}Sb_5(O,C)_5$ single crystals could not prove the presence of carbon atoms. A series of preparative experiments was carried out to reveal the role of carbon and purity of the *RE* elements on the formation of the $RE_9Sb_5O_4C$ and $RE_{9-\delta}Sb_5(O,C)_5$ phases.

Commercial-grade late rare earth metals (Gd–Lu) usually contain light-atom impurities including oxygen (ca. 1 atom-%), nitrogen (ca. 0.5 atom-%), hydrogen (ca. 3 atom-%) and carbon (ca. 1 atom-%).[18,19] Although no comparable literature data could be found for the light lanthanides, it is possible that the level of impurities is somewhat higher due to their stronger affinity to the light p-elements. Samples with a loading composition of $La_9Sb_5O_5$ (no added carbon) were prepared from both commercial-grade (ca. 93 atom-%) and purified La metals (Ames Laboratory, 99.9 atom-%). According to the X-ray powder analysis, $La_9Sb_5O_4C$ was the major phase (ca. 75 wt.-%, Figure 2, full triangles) in the sample made from the commercial La metal, whereas its amount in the sample with purified La metal was less than 14 wt.-% (Figure 2, $x = 0$, open circles). Similar results were obtained for the $Ho_9Sb_5O_5$ samples: the commercial Ho yielded 58% (Figure 2, full triangles), whereas the purified one gave only 13% of $Ho_{9-\delta}Sb_5(O,C)_5$ (Figure 2, $x = 0$, open diamonds). We do not know how much carbon is present in the commercial lanthanum and whether its amount is sufficient to yield 75 wt.-% of $La_9Sb_5O_4C$. If the amount of carbon is insufficient then potentially other impurities, although very unlikely, may stabilize these phases. Hydrogen is unlikely to be a factor, as the high temperatures and dynamic vacuum make Ta tubing transparent to hydrogen, thus allowing hydrogen to escape from the sample.[20] We believe that accidental carbon contamination during handling and preparation may be a factor.

The proof that carbon, and not other light elements, stabilizes the targeted phases comes from the series of experiments involving the purified La and Ho and controlled amounts of carbon in $RE_9Sb_5O_{5-x}C_x$ (Figure 2). The largest yield for the $RE_9Sb_5O_4C$ phases ($P4/n$) was achieved for the loading compositions with $x = 1$. Another important finding regards the composition of the $RE_{9-\delta}Sb_5(O,C)_5$ phases. The sintered $Ho_9Sb_5O_{4.5}C_{0.5}$ sample contained the $Ho_{9-\delta}Sb_5(O,C)_5$ phase with a high yield (99 wt.-%), which suggests that the O/C ratio in some $RE_{9-\delta}Sb_5(O,C)_5$ phases may be close to 4.5:0.5 (or 9:1). As discussed before, the O/C ratio is likely to be variable ($4:1 < \text{O/C ratio} \leq 9:1$). The amount of carbon retained in this series of phases is, however, unlikely to exceed 1, since the samples with $x > 1$ were less pure, as shown in Figure 2.

Conclusion

In the process of resolving the compositions of the $RE_9Sb_5O_4C$ phases, the novel phases $RE_{9-\delta}Sb_5(O,C)_5$ and $La_{14}Sb_8O_7C$ (*RE* = La, Ho) were discovered. All belong to a family of natural superlattice phases based on the intergrowth of NaCl-type *RE*Sb slabs and *RE*–O–C layers. The pivotal role of carbon in the formation of these phases has been clearly demonstrated. It has also been shown that the purity of rare earth elements dictates the outcome of the synthesis.

Although the O/C ratio and the positions of the oxygen and carbon atoms could be unambiguously established in the $RE_9Sb_5O_4C$ phases from the single-crystal X-ray and bond valence analyses, the exact O/C ratio could not be reliably refined for the other two phases. Still, it appears that all phases tend to be charge-balanced and the O/C ratio dictates both the *RE* content and the atomic arrangement within the *RE*–O–C layers. The most carbon-rich phases are $RE_9Sb_5O_4C$, and further carbon incorporation was unsuccessful. Lowering the carbon content results in $RE_{9-\delta}Sb_5(O,C)_5$ phases with an O/C ratio larger than 4:1, and in $La_{14}Sb_8O_7C$ with an O/C ratio of 7:1.

The layered nature of these phases suggests that other structures may be formed, for example, with *RE*Bi slabs instead of *RE*Sb ones, or with thicker *RE*Sb slabs. Currently, the research efforts are conducted to test these ideas.

Experimental Section

Synthesis: The rare earth antimonide oxide/oxycarbide samples were prepared from antimony metal (99.999 wt.-%, CERAC Inc.), La_2O_3 and Ho_2O_3 powders (99.99 wt.-%, Rhône–Poulenc) and carbon powder (99.995 wt.-%, Alfa Aesar). Rare earth metals with different levels of purity, including the commercial-grade *RE* metal (ca. 93 atom-%, CERAC Inc.) and the *RE* metals purified by Ames Laboratory (99.9 atom-%), were used for parallel syntheses and analyses. The general synthetic schemes involved three steps. As the first step, *RE*Sb binaries were prepared by direct sintering of the elements. Mixtures of rare earth metal filings and ground elemental antimony in a 1:1 atomic ratio were pressed into 1 g pellets in a glove box. The samples were sealed in evacuated silica tubes 10–15 cm in length, then heated to 600 °C at a rate of 50 °C/h. The sintering temperature was maintained at 600 °C to allow the antimony to react with the rare earth metal. After 12 h, the temperature was raised to 850 °C at a rate of 50 °C/h and kept for 48 h to drive the reaction to completion. Black pellets were obtained after cooling in air. The purity of these binaries was confirmed by X-ray powder diffraction analysis. The second step involved preparing the pseudo compounds "RE_4O_5" and "RE_4O_4C" from a stoichiometric amount of *RE* metal filings, calcined RE_2O_3 powders, and carbon powder. The mixtures were pressed into 0.5 g pellets under argon. Subsequently, the sample pellets were sintered in evacuated silica tubes at 1000 °C for 48 h. Uniform black pellets were obtained after cooling. The products were air-sensitive; therefore, they were handled and stored in a glove box. Finally, the precursors were mixed in different ratios according to:

$5\ RE\text{Sb} + (1 - x)\ \text{"}RE_4O_5\text{"} + x\ \text{"}RE_4O_4C\text{"} = RE_9Sb_5O_{5-x}C_x$ ($x = 0$, 0.5, and 1)

Samples with a total weight of 0.3 g were pressed into pellets and sealed in Ta tubes under argon. The Ta tubes were placed into a molybdenum susceptor and heated in a high-frequency induction

Table 3. Annealing temperature, carbon content, and product appearances of the $RE_9Sb_5O_{5-x}C_x$ samples.

	T [°C]	General formula	A (x = 0) Commercial-grade *RE* metal	B (x = 0)	C (x = 0.5)	D (x = 1)	E (x = 1) With extra 0.5 mol of carbon
1	1400	$La_9Sb_5O_{5-x}C_x$	–	–	–	sintered	–
2	1550	$La_9Sb_5O_{5-x}C_x$	molten	molten	molten	molten	molten
3	1650	$Ho_9Sb_5O_{5-x}C_x$	sintered	sintered	sintered	sintered	molten
4	1575	$Ho_9Sb_5O_{5-x}C_x$ + 0.3 Ho_5Sb_3	–	–	–	molten	–

furnace under a dynamic vacuum below 10^{-5} Torr. The reaction temperature was monitored by an optical pyrometer. All samples were annealed at the desired temperature for 8 h, and then left to cool to room temperature under dynamic vacuum. The products obtained either remained in a pellet form or were solidified from a melt. All samples appeared to be dark gray in color with a metallic luster. The La samples were sensitive to air and decomposed into a white/gray powder; the Ho samples were stable in air. Twelve samples were prepared according to the general synthetic procedures. As shown in Table 3, these samples can be placed into five groups according to the synthetic conditions and purity of the rare earth elements. Samples labeled B, C, D, and E (Table 3) were prepared from high-purity *RE* metals. Samples A were produced to illustrate the impact of impurities in commercial-grade *RE* metals. Lastly, samples E were synthesized with additional carbon to determine the maximum amount of carbon that can be retained in the system.

Single-Crystal X-ray Diffraction and Structure Refinement: Single-crystal X-ray diffraction studies were performed on crystals extracted from the crushed samples. Room-temperature diffraction data were collected with a STOE IPDSII diffractometer by using Mo-K_α radiation in the whole reciprocal sphere. A numerical absorption correction was based on the crystal shape that was originally derived from the optical face indexing but was later optimized against equivalent reflections by using the STOE X-Shape software.[21] The data for the $La_{8.80(1)}Sb_5(O,C)_5$ and $La_{14}Sb_8O_7C$ single crystals were collected with a Bruker SMART Apex II CCD diffractometer (Mo-K_α radiation) at 100(2) K in a reciprocal hemisphere. Intensities were extracted and then corrected for Lorentz and polarization effects through the SAINT program.[22] Numerical absorption correction was based on the crystal shape obtained from the optical face indexing. Structural determinations and refinements of all the data sets were performed by using the SHELXL program.[23] Crystal structures were determined for five new phases. These new compounds are identified by their refined compositions and space groups as follows: $La_{14}Sb_8O_7C$ with *P*4*bm* symmetry, $La_{8.80(1)}Sb_5(O,C)_5$ and $Ho_{8.84(3)}Sb_5(O,C)_5$ with *P*4/*nmm* symmetry, $La_9Sb_5O_4C$ and $Ho_9Sb_5O_4C$ with *P*4/*n* symmetry. The crystallographic information of $La_{14}Sb_8O_7C$, $La_{8.80(1)}Sb_5(O,C)_5$, $Ho_{8.84(3)}Sb_5(O,C)_5$, $La_9Sb_5O_4C$ and $Ho_9Sb_5O_4C$ is given in Tables 4 and 5. Further details of the crystal structure investigations can

Table 4. Crystallographic data and refinement results for the $La_{14}Sb_8O_7C$, $La_{8.80}Sb_5(O,C)_5$, $La_9Sb_5O_4C$, $Ho_{8.84}Sb_5(O,C)_5$, and $Ho_9Sb_5O_4C$ single crystals (Mo-K_α radiation).

Sample code[a]	2B	1D	2D	3C	4D
Refined composition	$La_{14}Sb_8O_7C$	$La_{8.80(1)}Sb_5(O,C)_5$[b]	$La_9Sb_5O_4C$	$Ho_{8.84(3)}Sb_5(O,C)_5$[b]	$Ho_9Sb_5O_4C$
Formula mass	3042.75	1911.16	1934.95	2148.38	2169.13
Temperature [K]	100(2)	100(2)	293(2)	100(2)	293(2)
Space group	*P*4*bm*	*P*4/*nmm*	*P*4/*n*	*P*4/*nmm*	*P*4/*n*
Unit-cell dimensions [Å]	13.0788(1)	4.623(1)	10.414(2)	4.3628(2)	9.782(1)
	9.3886(2)	9.388(2)	9.334(2)	8.8084(7)	8.768(1)
Volume [Å^3]	1605.97(4)	200.63(5)	1012.2(3)	167.659(7)	838.94(1)
Z	4	0.40	2	0.40	2
$D_{calcd.}$ [g cm^{-3}]	6.292	6.327	6.349	8.462	8.587
Abs. coeff. [mm^{-1}]	24.641	24.878	25.063	48.760	49.763
F(000)	2526	319	1612	353	1792
Crystal size [mm]	0.062 × 0.039 × 0.015	0.090 × 0.069 × 0.054	0.023 × 0.015 × 0.006	0.027 × 0.021 × 0.019	0.048 × 0.041 × 0.029
θ range [°]	3.09–52.22	2.17–45.21	3.52–34.74	4.63–44.94	2.32–29.23
Index ranges	$-26 \le h \le 28$,	$-9 \le h \le 8$,	$-16 \le h \le 15$,	$-8 \le h \le 7$,	$-13 \le h \le 10$,
	$-19 \le k \le 29$,	$-9 \le k \le 8$,	$-16 \le k \le 16$,	$-8 \le k \le 7$,	$-13 \le k \le 13$,
	$-18 \le l \le 20$	$-17 \le l \le 16$	$-14 \le l \le 14$	$-17 \le l \le 14$	$-10 \le l \le 11$
Reflections collected	33821	5866	21750	3101	5452
Independent reflections	8703	520	2112	456	1142
R_{int}	0.1029	0.0359	0.1163	0.2166	0.0859
Completeness to max. 2θ	98.2%	95.6%	96.4%	99.8%	99.4%
Data/restraints/param.	8703/1/83	520/0/17	2112/0/47	456/0/17	1142/0/47
Goodness-of-fit on F^2	1.007	1.044	1.083	0.908	0.760
Final R indices [$I > 2\sigma(I)$]	$R1$ = 0.0570	$R1$ = 0.0184	$R1$ = 0.0531	$R1$ = 0.0481	$R1$ = 0.0263
	$wR2$ = 0.1036	$wR2$ = 0.0359	$wR2$ = 0.0902	$wR2$ = 0.1045	$wR2$ = 0.0421
R indices (all data)	$R1$ = 0.1084,	$R1$ = 0.0245,	$R1$ = 0.1027,	$R1$ = 0.0642,	$R1$ = 0.0596,
	$wR2$ = 0.1233	$wR2$ = 0.0372	$wR2$ = 0.1024	$wR2$ = 0.1081	$wR2$ = 0.0469
Extinction coefficient	0.00007(2)	0.0046(5)	0.00046(6)	0.0040(9)	0.00103(4)
Diffr. peak/hole [e Å^{-3}]	6.200/–5.423	1.239/–1.860	4.056/–3.991	3.452/–6.895	1.946/–2.557

[a] Sample codes refer to the synthetic conditions listed in Table 3. [b] Composition refined with oxygen atoms occupying all interstitial sites, since the ratio of O and C could not be determined unambiguously.

Table 5. Atomic and isotropic temperature (U) parameters for the $La_{14}Sb_8O_7C$, $La_{8.80}Sb_5(O,C)_5$, $La_9Sb_5O_4C$, $Ho_{8.84}Sb_5(O,C)_5$, and $Ho_9Sb_5O_4C$ single crystals.

Atom	Site	Occupancy	x/a	y/b	z/c	U [Å^2]
			$La_{14}Sb_8O_7C$, 100(2) K			
La(1)	2*a*	1	0	0	0.0188(2)	0.0040(2)
La(2)	2*b*	1	0	1/2	0.0029(1)	0.0047(1)
La(3)	4*c*	1	0.24915(3)	0.25085(3)	0.00983(8)	0.0042(1)
La(4)	4*c*	1	0.10905(3)	0.60905(3)	0.3462(1)	0.00448(8)
La(5)	8*d*	1	0.99027(4)	0.24992(4)	0.69143(5)	0.00427(7)
La(6)	8*d*	1	0.15480(3)	0.88289(3)	0.3529(1)	0.00418(5)
Sb(1)	2*a*	1	0	0	0.6582(1)	0.0044 (2)
Sb(2)	2*b*	1	0	1/2	0.6464(1)	0.0047(2)
Sb(3)	4*c*	1	0.23992(4)	0.26008(4)	0.65386(9)	0.0049(1)
Sb(4)	8*d*	1	0.00157(4)	0.75143(4)	0.04785(7)	0.0041(1)
O(1)	2*b*	1	0	1/2	0.239(1)	0.008(2)
O(2)	4*c*	1	0.2387(5)	0.7387(5)	0.262(1)	0.007(1)
O(3)	8*d*	1	0.2390(4)	0.0271(4)	0.4393(7)	0.0066(8)
C(1)	2*a*	1	0	0	0.278(1)	0.0013(2)
			$La_{8.80(1)}Sb_5(O,C)_5$, 100(2) K			
La(1)	2*c*	1	1/4	1/4	0.3405(1)	0.0075(1)
La(2)	8*i*	0.1897(7)	3/4	0.1810(2)	0.9972(2)	0.0175(2)
Sb(1)	2*c*	1	1/4	1/4	0.6974(1)	0.0074(1)
O(1)[a]	2*c*	1	1/4	1/4	0.0889(7)	0.045(2)
			$Ho_{8.84(3)}Sb_5(O,C)_5$, 100(2) K			
Ho(1)	2*c*	1	1/4	1/4	0.33855(7)	0.0122(2)
Ho(2)	8*i*	0.192(1)	3/4	0.1905(8)	0.999(2)	0.025(1)
Sb(1)	2*c*	1	1/4	1/4	0.6933(1)	0.0122(2)
O(1)[a]	2*c*	1	1/4	1/4	0.086(2)	0.051(5)
			$La_9Sb_5O_4C$, 293(2) K			
La(1)	2*c*	1	1/4	1/4	0.6663(2)	0.0071(3)
La(2)	8*g*	1	0.3535(1)	0.9536(1)	0.3460(1)	0.0069(1)
La(3)	8*g*	1	0.1692(1)	0.0219(1)	0.0020(1)	0.0076(1)
Sb(1)	2*c*	1	1/4	1/4	0.3070(3)	0.0108(4)
Sb(2)	8*g*	1	0.3471(1)	0.9472(1)	0.7018(1)	0.0072(1)
O(1)	8*g*	1	0.3722(8)	0.9727(9)	0.092(1)	0.010(2)
C(1)	2*c*	1	1/4	1/4	0.929(3)	0.011(4)
			$Ho_9Sb_5O_4C$, 293(2) K			
Ho(1)	2*c*	1	1/4	1/4	0.6713(2)	0.0104(3)
Ho(2)	8*g*	1	0.3540(1)	0.9547(1)	0.3443(1)	0.0096(1)
Ho(3)	8*g*	1	0.1682(1)	0.0233(1)	0.0022(1)	0.0094(1)
Sb(1)	2*c*	1	1/4	1/4	0.3155(3)	0.0125(4)
Sb(2)	8*g*	1	0.3458 (1)	0.9455(1)	0.6986(1)	0.0094(2)
O(1)	8*g*	1	0.3699(6)	0.9740(8)	0.090(1)	0.011(2)
C(1)	2*c*	1	1/4	1/4	0.931(4)	0.016(6)

[a] Atomic sites that were expected to be occupied by a mixture of O and C.

be obtained from the Fachinformationszentrum Karlsruhe, 76344 Eggenstein-Leopoldshafen, Germany (Fax: +49-7247-808-666; E-mail: crysdata@fiz.karlsruhe.de) on quoting the depository numbers CSD-422097 (for $La_{14}Sb_8O_7C$), -422098 [for $La_{8.80(1)}Sb_5(O,C)_5$], -422099 (for $La_9Sb_5O_4C$), -422095 [for $Ho_{8.84(3)}Sb_5(O,C)_5$], and -422096 (for $Ho_9Sb_5O_4C$).

X-ray Powder Diffraction: The sintered samples were subjected to X-ray powder diffraction analyses. Between 20 and 50 mg of sample were used for each data collection. Diffraction data in the 20–70° 2θ range were collected with a PANalytical X'Pert Pro diffractometer with an X'Celerator detector and Cu-$K_{\alpha 1}$ radiation. From the X-ray powder pattern, the desired phase in each sample was identified along with the side products. The full-profile Rietveld refinement (Rietica program)[24] was used to refine the lattice constants and the amount of side products. The structural models obtained from single-crystal X-ray diffraction studies were used for the Rietveld refinement. The $La_{9-\delta}Sb_5(O,C)_5$, $Ho_{9-\delta}Sb_5(O,C)_5$, $La_9Sb_5O_4C$, and $Ho_9Sb_5O_4C$ phases were identified in the bulk samples. The extracted lattice constants, purity, and corresponding side products are listed in the Supporting Information with the sample codes representing the synthetic conditions given in Table 3.

Supporting Information (see footnote on the first page of this article): Crystal-structure details, evidence of structural anomalies, results from X-ray powder diffraction, and analyses of the formation of side products.

Acknowledgments

This work was supported by a Discovery Grant from the Natural Sciences and Engineering Research Council of Canada and by a grant from the ACS Petroleum Research Fund.

[1] K. Koumoto, I. Terasaki, R. Funahashi, *MRS Bull.* **2006**, *31*, 206.
[2] F. J. Disalvo, *Science* **1999**, *285*, 703.
[3] G. J. Snyder, E. S. Toberer, *Nat. Mater.* **2008**, *7*, 105.
[4] F. Gascoin, S. Ottensmann, D. Stark, S. M. Haile, G. J. Snyder, *Adv. Funct. Mater.* **2005**, *15*, 1860.
[5] J. Nuss, M. Jansen, *Acta Crystallogr., Sect. B* **2007**, *63*, 843.
[6] J. Nuss, H. G. von Schnering, Y. Grin, *Z. Anorg. Allg. Chem.* **2004**, *630*, 2287.
[7] J. Nuss, M. Jansen, *Z. Kristallogr. New Cryst. Struct.* **2009**, *224*, 11.
[8] D. X. Li, Y. Haga, H. Shida, T. Suzuki, Y. S. Kwon, *Phys. Rev. B* **1996**, *54*, 10483.
[9] G. S. Nolas, J. L. Cohn, B. C. Chakoumakos, G. A. Slack, *Therm. Conduct.* **2000**, *25*, 122.
[10] R. Gaume, B. Viana, D. Vivien, J.-P. Roger, D. Fournier, *Appl. Phys. Lett.* **2003**, *83*, 1355.
[11] P. Wang, S. Forbes, T. Kolodiazhnyi, K. Kosuda, Y. Mozharivskyj, *J. Am. Chem. Soc.* **2010**, *132*, 8795.
[12] D. W. Jones, I. J. McColm, R. Steadman, J. Yerkess, *J. Solid State Chem.* **1984**, *53*, 376.
[13] D. W. Jones, I. J. McColm, J. Yerkess, *J. Solid State Chem.* **1991**, *92*, 301.
[14] Z. Sarbak, *Binary Rare Earth Oxides* (Eds.: G. Adachi, N. Imanaka, Z. C. Kang), Kluwer Academic Publishers, Dordrecht, The Netherlands, **2005**, vol. 84.
[15] I. D. Brown, D. Altermatt, *Acta Crystallogr., Sect. A* **1984**, *40*, C444.
[16] M. Atoji, *J. Chem. Phys.* **1981**, *74*.
[17] N. E. Brese, M. O'Keeffe, *Acta Crystallogr., Sect. B* **1991**, *47*, 192.
[18] D. Fort, V. K. Pecharsky, K. A. Gschneidner, *J. Alloys Compd.* **1995**, *226*, 190.
[19] S. Y. Dan'kov, A. M. Tishin, V. K. Pecharsky, K. A. Gschneidner, *Phys. Rev. B* **1998**, *57*, 3478.
[20] E. A. Leon-Escamilla, J. D. Corbett, *Chem. Mater.* **2006**, *18*, 4782.
[21] *X-Shape*, STOE & Cie. GmbH, Darmstadt, **2004**.
[22] *SAINT*, v6.02, Bruker AXS Inc., Madison, WI, **2002**.
[23] G. M. Sheldrick, *Acta Crystallogr., Sect. A* **2008**, *64*, 112.
[24] B. A. Hunter, C. J. Howard, *Rietica*, Australian Nuclear Science and Technology Organization, Menai, Australia, **2000**.

Received: March 25, 2011
Published Online: August 2, 2011

